

Sea Ice Concentration Analyses for the Baltic Sea and Their Impact on Numerical Weather Prediction

MATTHIAS DRUSCH

European Centre for Medium-Range Weather Forecasts, Reading, United Kingdom

(Manuscript received 23 February 2005, in final form 12 November 2005)

ABSTRACT

Sea ice concentration plays a fundamental role in the exchange of water and energy between the ocean and the atmosphere. Global real-time datasets of sea ice concentration are based on satellite observations, which do not necessarily resolve small-scale patterns or coastal features. In this study, the global National Centers for Environmental Prediction (NCEP) 0.5° sea ice concentration dataset is compared with a regional high-resolution analysis for the Baltic Sea produced 2 times per week by the Swedish Meteorological and Hydrological Institute (SMHI). In general, the NCEP dataset exhibits less spatial and temporal variability during the winter of 2003/04. Because of the coarse resolution of the NCEP dataset, ice extent is generally larger than in the SMHI analysis. Mean sea ice concentrations derived from both datasets are in reasonable agreement during the ice-growing and ice-melting periods in January and April, respectively. For February and March, during which the sea ice extent is largest, mean sea ice concentrations are lower in the NCEP dataset relative to the SMHI product. Ten-day weather forecasts based on the NCEP sea ice concentrations and the SMHI dataset have been performed, and they were compared on the local, regional, and continental scales. Turbulent surface fluxes have been analyzed based on 24-h forecasts. The differences in sea ice extent during the ice-growing period in January cause mean differences of up to 30 W m^{-2} for sensible heat flux and 20 W m^{-2} for latent heat flux in parts of the Gulf of Bothnia and the Gulf of Finland. The comparison between spatially aggregated fluxes yields differences of up to 36 and 20 W m^{-2} for sensible and latent heat flux, respectively. The differences in turbulent fluxes result in different planetary boundary height and structure. Even the forecast cloud cover changes by up to 40% locally.

1. Introduction

Sea ice concentration (CI) is a key parameter in the exchange processes between the ocean and the atmosphere. It strongly influences albedo, surface fluxes of latent and sensible heat, and the surface wind drag. The exchange processes between ice-covered ocean surfaces and the atmosphere have been studied on various spatial and temporal scales covering decadal modes (e.g., Hurrell et al. 2003; Deser et al. 2002), annual and seasonal variability (e.g., Deser et al. 2000; Slonosky et al. 1997), and day-to-day variations (e.g., Brümmer et al. 2002; Launiainen et al. 2001).

Because open water and ice-covered water have completely different albedo characteristics and surface roughness, the radiation and energy balances and con-

sequently the turbulent fluxes of momentum and heat at the surface will be distinctly different. Different surface fluxes will eventually cause differences in the local low-level wind, temperature, and humidity fields and in the planetary boundary layer height and low cloud cover. The spatial distribution of sea ice concentration can also influence the atmospheric conditions on the regional scale. Andersson and Gustafsson (1994) analyzed the synoptic situation on 11–12 January 1987, during which intense convective snowbands formed over the Baltic Sea during a cold easterly flow over northwestern Europe. They found that the Finnish and Swedish coastlines and the ice borders along these coasts had the largest effect on the structure, intensity, and position of the major snowbands.

Real-time sea ice concentration and sea surface temperature (SST) information is of fundamental importance for weather centers as observations for the analyses or as analysis products that can be used directly for the initialization of the forecast. At the European Cen-

Corresponding author address: Matthias Drusch, ECMWF, Shinfield Park, Reading RG2 9AX, United Kingdom.
E-mail: dar@ecmwf.int

tre for Medium-Range Weather Forecasts (ECMWF), CI and SST fields are obtained through the National Centers for Environmental Prediction (NCEP). The SST fields are based on in situ observations from ships and buoys and on satellite data, mainly obtained in the infrared spectral range. The spatial resolution of these sensors is higher than the resolution of a global NWP model, and in the near future 10-km SST analysis datasets will be available through the Global Ocean Data Assimilation Experiment (GODAE) High-Resolution Sea Surface Temperature Pilot Project (GHRSSST-PP). NCEP's sea ice concentration data have been derived from the Special Sensor Microwave Imager (SSM/I) using a tie-point algorithm as described in Campbell et al. (1976) and Cavalieri et al. (1984). The spatial resolution of passive microwave radiometers is comparably coarse, and measurements at low frequencies (i.e., 19–37 GHz) can be contaminated in coastal areas and small basins by the influence of land (Lindau and Ruprecht 2000). Some NWP centers, for example, the Swedish Meteorological and Hydrological Institute (SMHI) and the Norwegian Meteorological Institute, produce high-resolution sea ice concentration analyses on the regional scale. For enclosed basins (in terms of sea ice) high-resolution limited-area datasets can be used to update the global NCEP product to provide a better estimate of the sea ice state in coastal areas.

To demonstrate the applicability of this approach, the high-resolution Baltic Sea ice concentration analysis from SMHI is used to replace the global NCEP product in the Baltic Sea. Two sets of 10-day forecast experiments have been performed to quantify the impact of sea ice concentration on weather parameters and the weather forecast in the Baltic Sea area and for northern Europe: 1) the control run based on the global NCEP analysis and 2) the experimental run using the high-resolution Baltic Sea analysis from the SMHI. The NCEP SST fields are used for both studies as the quality check. Both fields—SST and sea ice concentration—remain constant during the 10-day forecast period. There consequently is no feedback from the atmosphere to the ocean.

The Baltic Sea is of particular scientific interest, since the Baltic Sea Experiment (BALTEX) has become the European continental-scale experiment within the Global Energy and Water Cycle Experiment (GEWEX) of the World Climate Research Programme. For a detailed description of the project and an overview of related research the reader is referred to Raschke et al. (2001) and the *Boreal Environment Research* BALTEX Theme Issue I (2002, Vol. 7, No. 3) and BALTEX Theme Issue II (2002, Vol. 7, No. 4).

2. CI analysis datasets

In the operational Integrated Forecast System (IFS) at ECMWF, sea ice concentration and sea surface temperature analyses are based on the corresponding daily 0.5° datasets produced by NCEP. Both products are resampled from their original regular latitude–longitude grid to the reduced Gaussian model grid using bilinear interpolation. In coastal areas, where the bilinear interpolation method fails, the aggregation is based on the nearest sea grid boxes (as defined through NCEP's land/sea mask) and their distances to the actual model grid point. The analyses are performed every 6 h (for 0000, 0600, 1200, and 1800 UTC) after the atmospheric variational analysis is done. The first guess (i.e., the previous analysis) is only updated when new datasets are available. After the interpolation has been performed the following four empirically derived quality checks are applied for the CI analysis: 1) CI of less than 20% is set to 0%, 2) CI of greater than 100% is set to 100%, 3) if the SST is higher than 1°C , CI is set to 0%, and 4) grid boxes north of 82.5°N are set to 100%.

If the fraction of new ice or melted ice in the global sea ice concentration as computed from the current analysis and the previous day's analysis exceeds 0.2%, the CI analysis is stopped and the data are examined by an analyst. In the case of corrupted data, for example, missing SSM/I scans in the NCEP product, the first guess is used. If the data show reasonable sea ice concentrations, the analysis is accepted. Sections 2a and 2b briefly describe the NCEP CI dataset and the SMHI product.

a. NCEP global dataset

The global CI dataset is based on passive microwave observations from SSM/I (Hollinger et al. 1987). Brightness temperature grids for 19- and 37-GHz dual polarization are produced from the antenna temperatures using a 12-h window, before and after 0000 UTC of the current day. The data extraction program is run at 0830 local time in the U.S. eastern time zone, and, in general, 12 out of 14 orbits are included (Grumbine 1996). The actual sea ice concentrations are calculated from the daily composite brightness temperature grids by following the method of Cavalieri et al. (1991). The tie-point algorithm calculates the total, first-year, and multiyear sea ice concentrations from the microwave polarization ratio at 19 GHz and the spectral gradient ratio, which uses the vertically polarized 37- and 19-GHz brightness temperatures (Cavalieri et al. 1991). Last, a number of quality checks, including a modified weather filter (Gloersen and Cavalieri 1986) and polar

gap filling, are applied. The final quality-checked product is a global map at 0.5° resolution (Grumbine 1996).

The spatial resolution corresponds to the -3 -dB resolution of the radiometer, which is approximately $69 \times 43 \text{ km}^2$ at 19 GHz (Hollinger et al. 1987). It has been shown (e.g., Drusch et al. 1999), however, that only 50% of the information obtained through an individual observation from SSM/I originates from the -3 -dB area. The area that contributes 99% of the information to an SSM/I observation is 3 times the -3 -dB region (i.e., $\sim 210 \times 130 \text{ km}^2$ at 19 GHz). SSM/I measurements in coastal areas and small basins are consequently likely to be contaminated by land.

b. SMHI Baltic Sea dataset

At SMHI, sea ice concentration, sea ice thickness, and sea surface temperature are analyzed 2 times per week. The analysis is done manually by an analyst based on Advanced Very High Resolution Radiometer (AVHRR) data and in situ observations. The final maps are digitized and archived at 1-km (sea ice and thickness) and ~ 10 -km (SST) resolution. It is likely that errors in this product are introduced through clouds and the fact that the analysis might be carried out by different forecasters on different days. However, for the applications at ECMWF the sea ice data have been linearly averaged to the reduced Gaussian model grid; the quality checks as outlined above have been applied.

3. Intercomparison of sea ice extent for winter 2003/04

For the Baltic Sea, there are no independent in situ observations for sea ice concentration available that could be used to validate the NCEP and SMHI products. As already mentioned above, the area contributing to 19-GHz SSM/I measurements is $\sim 210 \times 130 \text{ km}^2$. Therefore, spatial variability of sea ice concentration will be underestimated at the horizontal resolution of NWP models, which is typically below $50 \times 50 \text{ km}^2$. In addition, the accuracy of the NCEP sea ice product is reduced by the influence of land on the measured brightness temperatures. With the large number of islands and small subbasins, there exists almost no $\sim 210 \times 130 \text{ km}^2$ area in the Baltic Sea that is not contaminated by land (Lindau and Ruprecht 2000). In contrast, the SMHI product is based on in situ observations and AVHRR data, which represent NWP model resolution very well; the SMHI product gives a more realistic description of the true sea ice state in the Baltic Sea than does the NCEP product at resolutions below $50 \times$

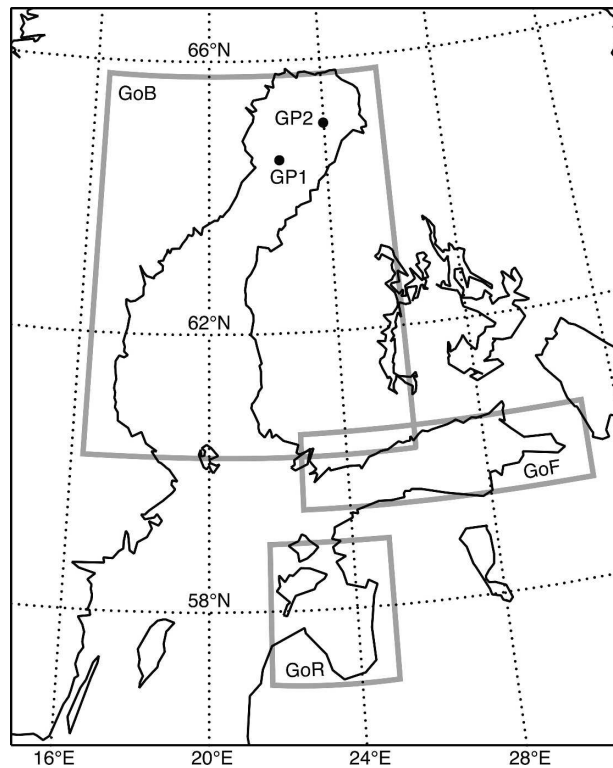


FIG. 1. The northern Baltic Sea area comprising the Gulf of Bothnia, the Gulf of Finland, and the Gulf of Riga. Also shown are the two grid points used to study local-scale impacts.

50 km^2 . To quantify the differences between both datasets the winter season of 2003/04 has been analyzed.

The sea ice analyses have been compared for the entire Baltic Sea and three different subbasins (Fig. 1): 1) the Gulf of Bothnia (GoB: 60.25° – 65.85°N , 16.5° – 26.0°E), 2) the Gulf of Finland (GoF: 59.5° – 60.6°N , 22.6° – 30.8°E), and 3) the Gulf of Riga (GoR: 56.9° – 59.0°N , 21.7° – 24.8°E). The mean sea ice concentrations for the four domains have been calculated from the analysis data on the reduced Gaussian model grid corresponding to T511 spectral resolution (~ 40 -km gridpoint separation). For the computation of sea ice extent in a specific region, the area covered by grid boxes with ice concentrations exceeding 20% has been divided by the total sea area. The 20% threshold is slightly higher than the 15% threshold that is commonly used in the literature (e.g., Alexander et al. 2004) and reflects the quality check in the CI analysis at ECMWF.

Time series for mean sea ice concentration and sea ice extent are shown in Fig. 2. In general, mean sea ice fractions calculated from the SMHI analysis and from the NCEP dataset are in reasonable agreement. In all

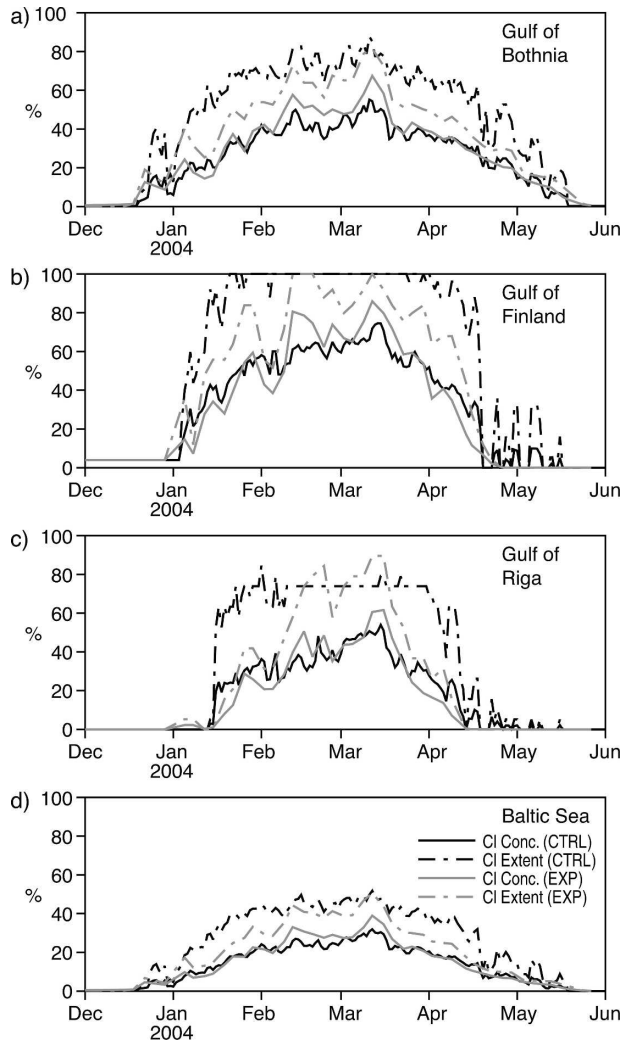


FIG. 2. Areal averaged sea ice extent (dashed lines) and sea ice concentration (solid lines) for winter 2003/04 for (a) GoB, (b) GoF, (c) GoR, and (d) the Baltic Sea. Values from the CTRL run (NCEP CI analysis) are shown in black; data from the EXP run (SMHI analysis) are presented in gray.

three subbasins the high-resolution SMHI dataset results in higher concentrations during the peak time of the ice season from mid-February to mid-March. For individual days, differences exceeding 20% can be found for the Gulf of Finland. During the growing and melting seasons, mean sea ice concentration from SMHI tends to be slightly smaller for the Gulf of Riga and the Gulf of Finland. The agreement between datasets for the Gulf of Bothnia is high.

The differences in sea ice extent are larger. In all three subregions, the two datasets can result in sea ice extents that differ by more than 30%. In general, the NCEP dataset leads to higher ice extents, which is due to the coarse resolution of the SSM/I satellite footprint.

For the Gulf of Riga, a plateau is obtained for the winter period from mid-February to the end of April. This plateau is an artifact of the interpolation of the coarse-resolution NCEP dataset to the limited number of model grid points in the array that defines the GoR region. For the Baltic Sea area, the differences in sea ice extent and sea ice concentration exceed 10% and 5%, respectively.

4. NWP application

The results presented in Fig. 2 show significant differences between the two CI analyses for the Baltic Sea and the three subbasins. To investigate the impact of the two different analyses on modeled surface parameters (e.g., turbulent fluxes of sensible and latent heat), the boundary layer, and eventually the quality of the medium-range weather forecasts, two experiments for the period from 5 January to 4 March have been performed using ECMWF's IFS: 1) the control run (CTRL) based on the global NCEP analysis and 2) the experimental run (EXP), in which the SMHI analysis is used for the Baltic Sea.

The following section gives a brief overview of the forecast system and the model physics that are most relevant for this study. The results for both experiments are compared and analyzed in the consecutive sections.

a. The Integrated Forecast System

The experiments are based on the IFS at T511 spectral resolution, which corresponds to grid points that are separated by ~40 km in the horizontal direction. The variables at each grid point, which are updated at each 15-min time step, are wind, temperature, humidity, cloud water and ice, cloud fraction, and also pressure at the surface grid points. The vertical resolution is 60 model levels between the earth's surface and 65 km. The lowest levels are at approximately 10, 30, 60, 100, and 160 m.

In the model, clouds are generated by large-scale ascent, cumulus convection, boundary layer turbulence, and radiative cooling. Cloud fraction and cloud water/ice content are forecast with their own prognostic equation. Interaction between clouds and radiation is based on radiative transfer computations for overcast and clear-sky conditions. Both components are weighted together according to the forecast cloud amount. At ECMWF, global atmospheric analyses are produced at 0000, 0600, 1200, and 1800 UTC by two four-dimensional variational data assimilation minimization cycles running from 0300 to 1500 and from 1500 to 0300 UTC. Ten-day forecasts are produced 2 times per day from the 0000 and 1200 UTC analyses.

Any model sea grid point can have two fractions: open water and ice. SST and sea ice concentration are defined through analyses, and both quantities are kept constant during the forecast. To describe the thermal interaction with the atmosphere, the sea ice is modeled as an ice slab discretized in four different layers, with open water underneath and a skin temperature for the thermal contact with the atmosphere. The total ice depth is fixed and there is no snow accumulation on the ice. Sea ice heat transfer is modeled following the Fourier law of diffusion, where the bottom boundary condition is the temperature of freezing water and the top boundary condition is the net heat flux at the surface obtained from the solution of the ice skin thermal budget (ECMWF 2003).

For the computation of the turbulent transports of momentum, heat, and moisture, the large-scale variables are used under the assumption that the transports are proportional to the vertical gradients. At the earth's surface, the turbulent fluxes of heat H and water vapor E are computed as a function of air–surface differences and surface characteristics:

$$H_i = -\rho_a |U_l| C_{H,i} (c_p T_L + gz_L - c_p T_{sk,i}) \quad \text{and} \quad (1)$$

$$E_i = -\rho_a |U_l| C_{H,i} [q_L - q_{sat}(T_{sk,i})], \quad (2)$$

where ρ_a is the air density; c_p is the specific heat of moist air; g is the acceleration of gravity; $|U_l|$, T_L , q_L , and z_L are the wind speed, temperature, humidity, and height of the lowest atmospheric model level, respectively; q_{sat} is the saturation specific humidity; T_{sk} is the skin temperature; and $C_{H,i}$ is the turbulent exchange coefficient. Subscript i indicates that H and E are calculated separately for the open-water and sea ice part, which may occur in a single grid box. For this study, positive fluxes are defined as upward. For a detailed description of the calculation of the stability-dependent exchange coefficients the reader is referred to ECMWF (2003).

The planetary boundary layer height is not a prognostic variable and has to be diagnosed from the model forecast following the bulk Richardson method as proposed by Troen and Mahrt (1986). The boundary layer height h_{bl} is defined as the level at which the bulk Richardson number, based on the difference between quantities at that level and the lowest model level, reaches the critical value $Ri_{cr} = 0.25$. The bulk Richardson number Ri_b has been computed from the following set of equations:

$$|\Delta U|^2 = (u_{hbl} - u_l)^2 + (v_{hbl} - v_l)^2, \quad (3)$$

$$\epsilon = (R_{vapor}/R_{dry}) - 1, \quad (4)$$

$$s_{v,l} = c_{p,dry} T_l (1 + \epsilon q_l) + gz_l, \quad (5)$$

$$s_{v,hbl} = c_{p,dry} T_{hbl} (1 + \epsilon q_{hbl}) + gz_{hbl}, \quad (6)$$

$$\Delta s = 8.5 c_{p,dry} u_* Q_{0v} / w_s, \quad (7)$$

$$w_s = (u_*^3 + 0.6gQ_{0v}h_{bl}/T)^{1/3} \quad \text{for unstable conditions,} \quad (8)$$

$$w_s = u_* \quad \text{for stable conditions, and} \quad (9)$$

$$Ri_b = h_{bl} \frac{2g(s_{v,hbl} - s_{v,l} - \Delta s)}{(s_{v,hbl} + s_{v,l} - gh_{bl} - gz_l)|\Delta U|^2}, \quad (10)$$

where u and v are the horizontal components of the wind vector, R_{vapor} and R_{dry} are the gas constants for water vapor and dry air, respectively, s_v is the virtual dry static energy, $c_{p,dry}$ is the specific heat at constant pressure for dry air, T is air temperature, q is specific humidity, u_* is the friction velocity, and Q_{0v} is the virtual temperature flux in the surface layer. The subscripts l and hbl indicate the lowest model level and the level at which $Ri_b = Ri_{cr}$, respectively. The boundary layer height is found by a vertical scan from the surface upward. Because the computation of w_s depends on h_{bl} , the upward scan is done twice: the first scan uses $h_{bl} = 1000$ m, and the second uses the result of the first scan. For more details on the boundary layer parameterizations, the reader is referred to ECMWF (2003).

b. Sea ice coverage and turbulent surface fluxes

The experiment period from 5 January to 5 March roughly covers the first half of the sea ice season in the northern Baltic Sea basins. During January, most of the sea ice is formed in the Gulf of Bothnia and the Gulf of Finland (Fig. 2). The spatial distribution of sea ice concentration is shown in Fig. 3. The data represent mean values for the period from 5 January to 24 January from the CTRL and the EXP runs as analyzed at 1200 UTC. In general, the gradients in sea ice concentration in CTRL are smaller when compared with the corresponding EXP values. In the northern part of the Gulf of Bothnia, sea ice concentration in CTRL hardly exceeds 60%, with a maximum value of 78%. The minimum sea ice concentration is 28% in the central northern part (at 64.4°N, 22.8°E). In contrast, the SMHI/EXP run uses 97% CI along the very northern coastline and a small almost ice free area of 3% (at 64.0°N, 22.4°E). These differences are primarily due to the coarse resolution of the satellite product and the contamination by land. The aggregation to the reduced Gaussian model grid hardly influences the CTRL CI values in this region, because the CI values for coastal grid points are based on one or two NCEP grid points only. Substantial differences in CI also occur along the eastern coast of Sweden north of 60°N and in the Gulf

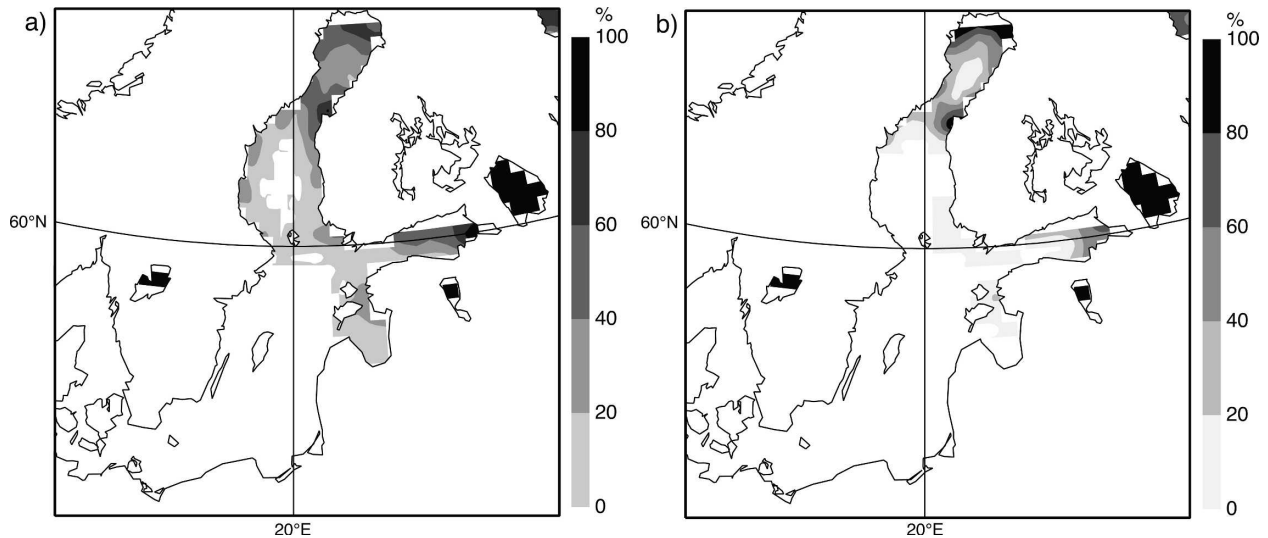


FIG. 3. Mean sea ice concentration for the study period of 5–24 Jan 2004: (a) NCEP/ECMWF (CTRL) and (b) SMHI/ECMWF (EXP).

of Finland, where an overestimation of low sea ice concentrations can be found in the CTRL run. The same holds for the Gulf of Riga, which is almost ice free in the EXP analysis. It has to be noted that these low ice concentrations originate from the temporal averaging only. In both individual analyses, the minimum ice concentration is 20% according to the quality checks in the NWP model.

The mean sea ice concentration fields in both experiments are becoming more similar when data from the entire experiment period are used. However, the temporal variability in the ice fields, that is, the field's standard deviation, is considerably higher in the SMHI-derived product. In both datasets, the largest temporal variability can be found in the Gulf of Bothnia around 64.5°N , 22.7°E and in the Gulf of Finland around 59.7°N , 26.4°E . The standard deviations for the GoB (GoF) are 36% (32%) and 26% (15%) for the EXP and CTRL experiments, respectively.

Based on the CTRL and EXP model runs, the turbulent surface fluxes for sensible and latent heat have been analyzed for the 2-month period starting on 5 January. Figures 4a,b show spatially integrated 24-h averages of latent and sensible heat fluxes from the CTRL run. The 24-h means have been computed from 24-h forecasts starting at 1200 UTC. The time series for the Baltic Sea and the three subbasins exhibit substantial temporal variability during the study period. In general, positive (upward) fluxes coincide with cold low-level temperatures caused by cold-air outbreaks.

The GoF and GoR regions are characterized by high upward fluxes of up to 85 W m^{-2} for latent heat and

100 W m^{-2} for sensible heat from 7 to 10 January. During this period, cold-air advection in the GoR, GoF, and the very eastern part of the Baltic Sea resulted in a strong spatial gradient in 2-m temperature. Temperatures at 1200 UTC were below -8°C in the Gulf of Riga and below -13°C in the Gulf of Finland. From 11 January onward, warm air moved eastward, reducing the surface fluxes. During this part of the study period, the turbulent fluxes in the three subbasins look similar. From 20 to 22 January, the entire Baltic Sea region was under the influence of colder air masses characterized by 1200 UTC 2-m temperatures in between -4° (central area) and -12°C in the Gulf of Finland. The strong vertical temperature gradient between the ocean and the atmosphere results in mean fluxes of up to 100 W m^{-2} (Fig. 4a). At the beginning of February, the entire Baltic Sea region was under the influence of warm air masses, again with temperatures of 6°C in the southern and central parts and from 4° to -3°C in the Gulf of Bothnia. Downward fluxes exceeding 50 W m^{-2} are obtained for the Gulf of Finland. In general, fluxes are smaller in GoB and GoF because of the presence of ice.

The mean values for the Baltic Sea obtained for January of 2004 agree reasonably well with long-term mean fluxes (1980–95) computed from the Comprehensive Ocean–Atmosphere Dataset (COADS). For January, Lindau (2002) obtained 50 and 35 W m^{-2} for latent heat and sensible heat, respectively. The corresponding values from the EXP run are 44 and 36 W m^{-2} . For February of 2004, the mean fluxes for the Baltic were found to be 4 W m^{-2} for sensible heat and 21 W m^{-2} for latent heat for both model runs. These values are con-

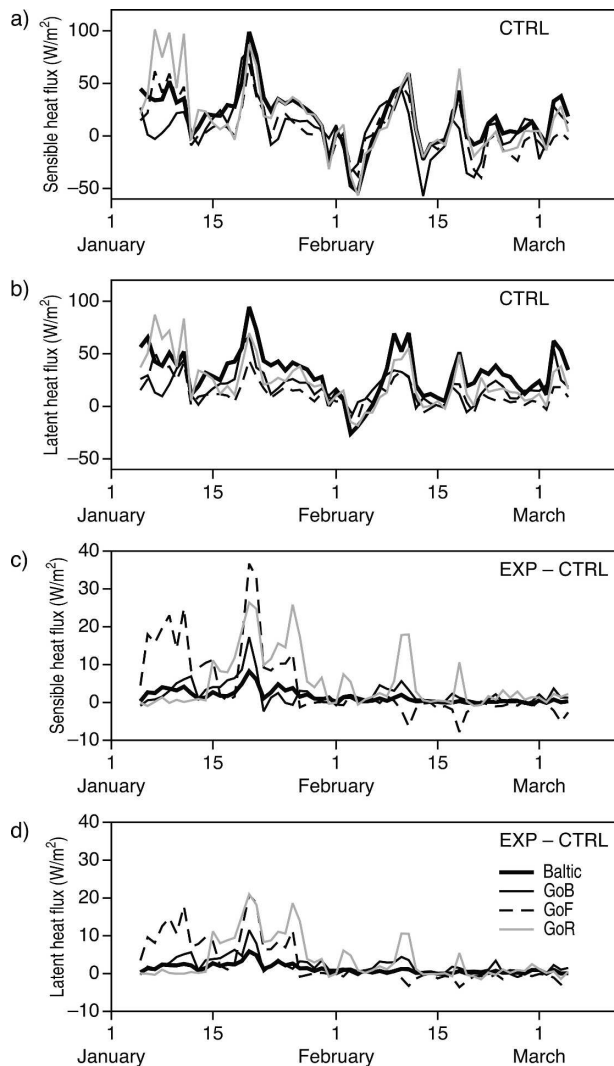


FIG. 4. Spatially integrated turbulent surface fluxes [(a) sensible heat flux and (b) latent heat flux] for 5 Jan–4 Mar 2004 as computed from the 24-h forecasts (1200 UTC base time) from the CTRL experiment. Also shown are the corresponding differences between EXP and CTRL for (c) sensible heat flux and (d) latent heat flux. Individual curves represent the Baltic Sea area (thick black), GoB (black), GoF (dashed), and GoR (gray).

siderably lower than the long-term means of 25 and 40 W m^{-2} for sensible and latent heat, respectively.

The differences between the EXP and CTRL runs are presented in Figs. 4c,d. For the GoR, where sea ice concentration is very low at the beginning of January in both analyses, the differences in fluxes do not exceed 2 W m^{-2} . During the second half of January, sea ice concentration increases (Fig. 2) and differences exceeding 25 W m^{-2} are obtained (Fig. 4c). The most pronounced differences are obtained for the GoF, where large fluxes and significant differences in CI are present. The difference of 36 W m^{-2} in sensible heat

flux, which is caused by differences in CI, is comparable to the temporal variability during the study period (Fig. 4a). For the GoB area, the two CI analyses result in spatially averaged flux differences of up to 16 W m^{-2} . In general, the largest differences between the EXP and CTRL runs can be found during cold airflow from the north or east when the turbulent heat fluxes from the sea to the air are largest. Open-water areas, which are present in the high-resolution CI dataset (EXP) but not in the SSM/I-derived product (CTRL), result in large fluxes. In late February and the beginning of March, when CI extent and concentration have reached their maximum values, the differences in both model runs are small. The differences in the heat fluxes between the EXP and the CTRL experiments are mainly positive (Figs. 4c,d). The results presented in Fig. 2 indicate that mean sea ice extent (or the extent of open water) rather than mean sea ice concentration is the determining influence on the fluxes.

To study the spatial pattern of the modeled turbulent fluxes, the 24-h mean values from the 1200 UTC 24-h forecast have been integrated in time. Results for the 5–24 January period, for which the temporal analysis exhibits the largest differences, are shown in Fig. 5. Sensible (Fig. 5a) and latent heat fluxes (Fig. 5b) are highly correlated. Maximum values are 68 and 75 W m^{-2} for the sensible and latent heat fluxes, respectively, in the southeastern part of the Baltic Sea. Under the presence of sea ice both fluxes are significantly reduced. In the northern part of the Gulf of Bothnia values from 6 to 24 W m^{-2} and from -9 to 26 W m^{-2} can be found for sensible and latent heat, respectively. The mean differences between the EXP and CTRL runs are shown in Figs. 5c,d. Again, sensible and latent heat fluxes are highly correlated. Coastal areas in the southern part of the Gulf of Bothnia and the central northern part of the Gulf of Bothnia, which are ice free in the EXP run but are at least partly ice covered in the CTRL run, show positive differences up to 30 W m^{-2} for the sensible heat flux and 20 W m^{-2} for the latent heat flux. However, along the Swedish and Finnish coastlines in the northern part of the GoB, local areas with high sea ice concentrations were identified through the SMHI analysis. These spots are characterized by reduced upward fluxes and can be identified by differences between the EXP and CTRL runs of up to -25 and -13 W m^{-2} for sensible and latent heat, respectively.

c. Regional sensible heat fluxes and planetary boundary layer height

Two days from the January experiment period have been selected to study the impact of the different ice analyses on the planetary boundary layer (PBL) on the

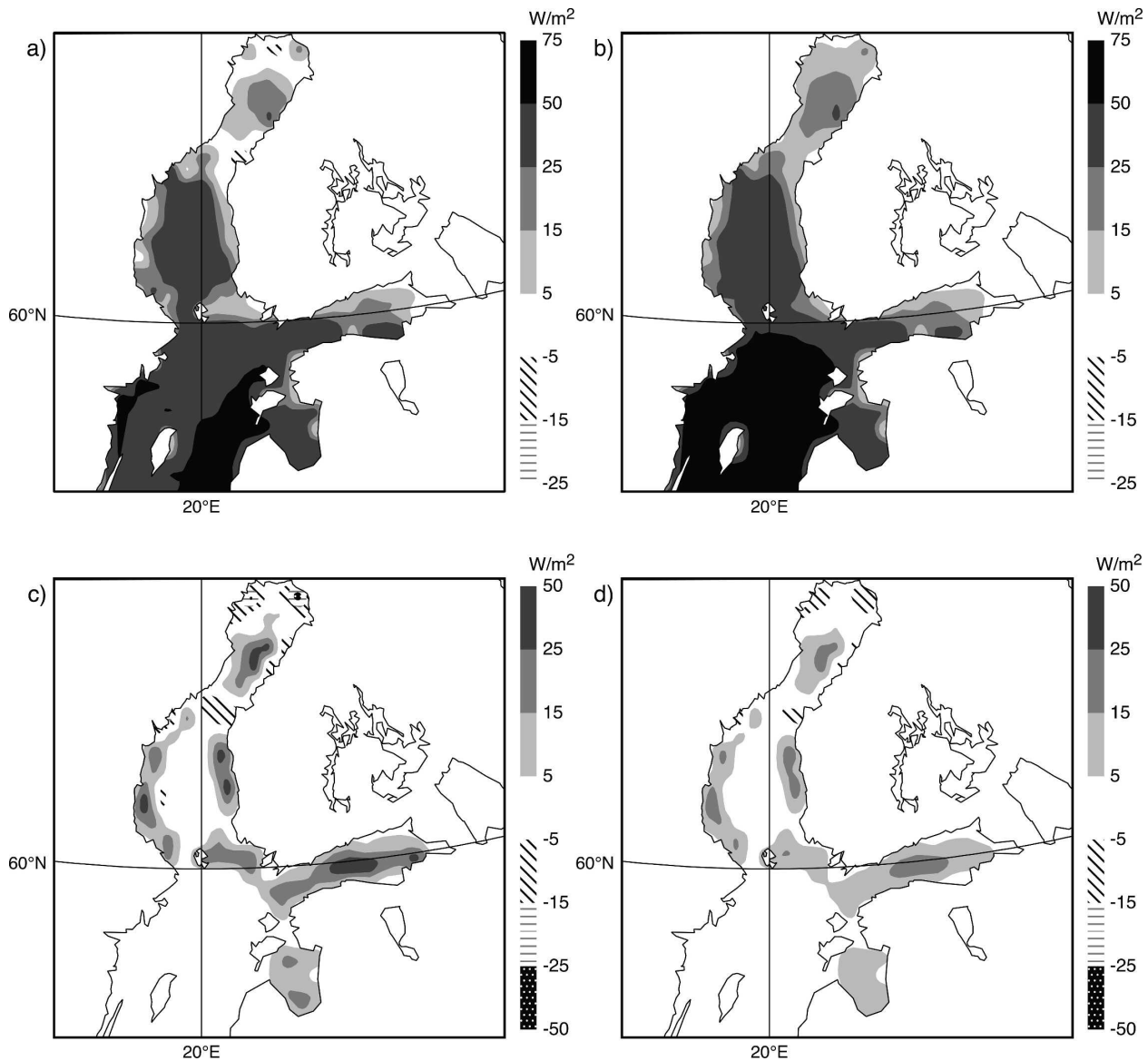


FIG. 5. Mean surface fluxes for 5–24 Jan 2004 as computed from the 24-h forecasts (1200 UTC base time) from the CTRL experiment for (a) sensible heat flux and (b) latent heat flux. Also shown are the differences EXP – CTRL for (c) sensible and (d) latent heat fluxes.

regional scale, namely, the Gulf of Bothnia and the Gulf of Finland, where the most significant changes occurred. On 12 January, the synoptic situation over this area was characterized by southeasterly winds with wind speeds ranging from 12 to 5 m s⁻¹ in the southern and northern part of the GoB, respectively. The corresponding 2-m air temperatures over large parts of this area ranged from 0° to -5°C. For this day, a high-resolution CI analysis was prepared by SMHI. The differences between the SMHI data and the operational product are negative for large parts of the northern GoB and the GoF. In the coastal areas of the northern

GoB the operational product yields considerably lower CI concentrations. These initial conditions as analyzed at 1200 UTC are summarized in Fig. 6a.

A northerly flow characterized 21 January, leaving the Gulf of Bothnia under the influence of cold air with 2-m temperatures varying from -14° to -7°C (Fig. 6b). For this day, the SMHI CI analysis leads to lower values relative to those of the SSM/I-derived NCEP product for most parts over the northern GoB. Only a small area in the central northern GoB remains ice free in the SMHI product.

The mean turbulent sensible heat flux differences for

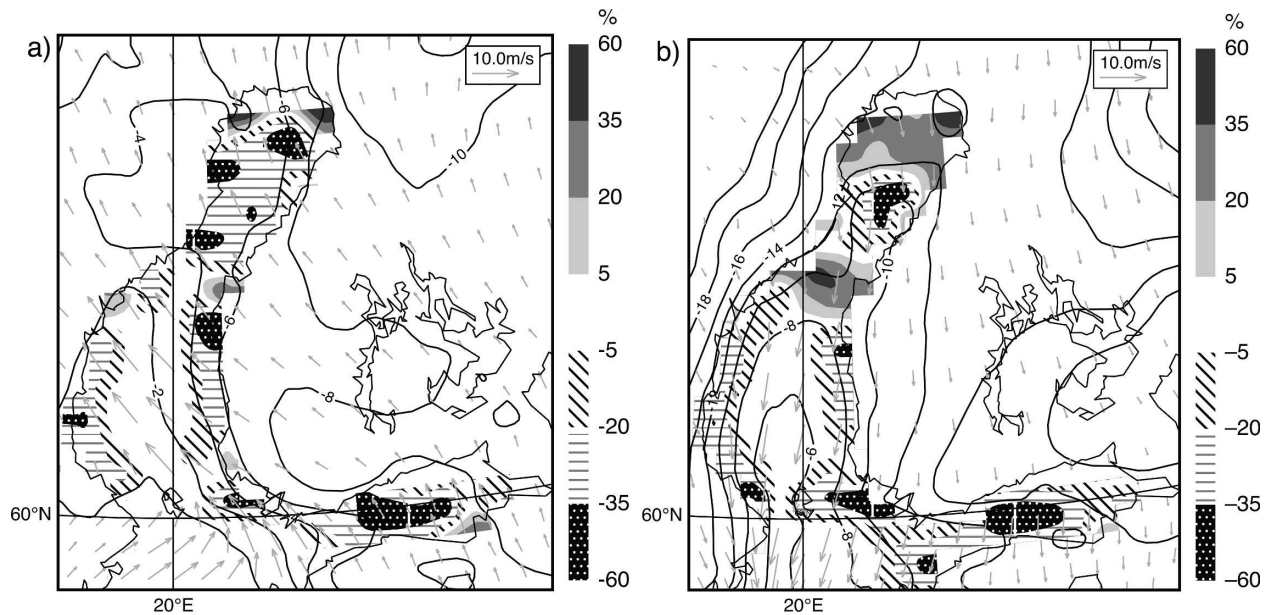


FIG. 6. Initial conditions for the forecasts from (a) 12 and (b) 21 January as analyzed at 1200 UTC. Temperature (2 m), wind speed (10 m), and the differences in CI concentration between the EXP run and the CTRL experiment are shown as isotherms ($^{\circ}\text{C}$), arrows (m s^{-1}), and shaded field (%), respectively.

the 6-h forecast period from 1200 UTC onward between the EXP run and the CTRL experiment are shown for 12 and 21 January (Fig. 7). As already discussed, lower CI concentrations in the SMHI product result in higher upward fluxes relative to those of the operational product and vice versa. The corresponding

differences in the forecast planetary boundary layer height at 1800 UTC are shown as contour lines. In general, an increase in sensible heat flux results in deeper planetary boundary layers. As a consequence, the differences between the EXP and CTRL runs in the sensible heat flux are positively correlated with the differ-

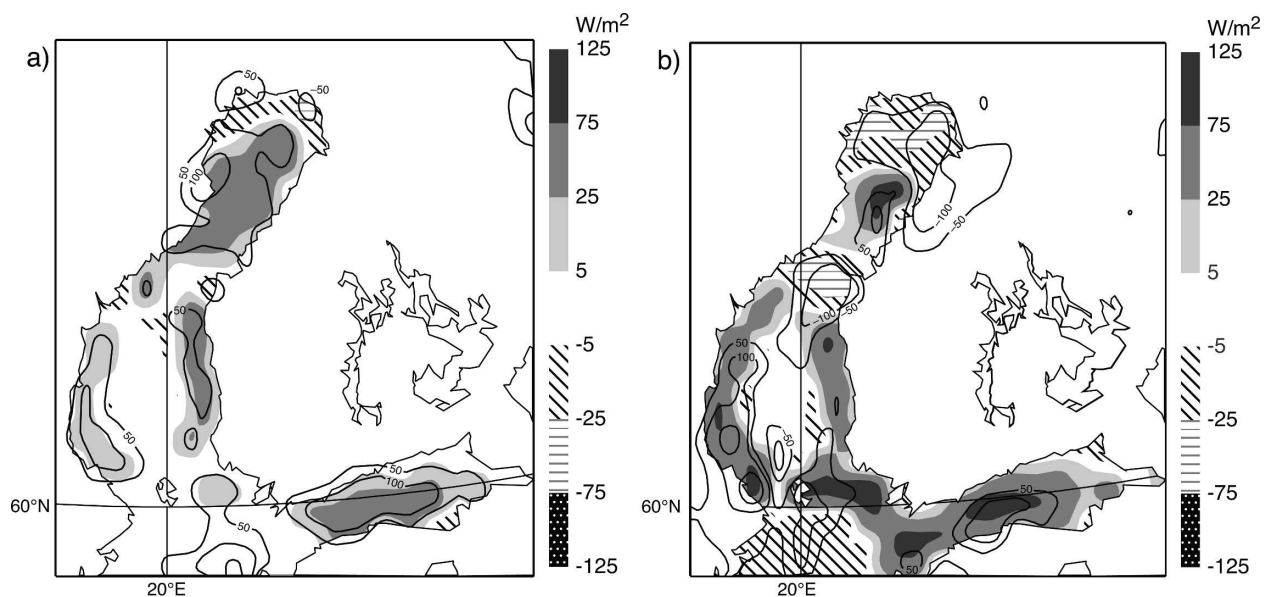


FIG. 7. Differences in sensible heat flux and planetary boundary layer height calculated from the CTRL experiment and the EXP run. The fields show 6-hourly forecasts based on (a) 12 and (b) 21 January analyses at 1200 UTC, respectively. The PBL height-difference (m) contours show 50-m increments. The differences in sensible heat flux are shown as shaded areas.

ences in the PBL height. In areas with flux differences larger than 25 W m^{-2} the differences in PBL height exceed 100 m. This amount is substantial relative to the absolute values, which are well below 500 m in the northern GoB. It is interesting to notice that the model appears to advect PBL height. For 21 January, the maximum differences in PBL height are located south of the maximum differences in sensible heat flux. In the 12 January figure, the northward displacement is slightly smaller but can still be detected in the GoF and the northern GoB region.

d. Local changes in the planetary boundary layer

To analyze the impact of different CI analyses on the local scale, two grid points have been selected. The points are located at $64.4^\circ\text{N}, 22.4^\circ\text{E}$ (GP1) and $65.1^\circ\text{N}, 24.0^\circ\text{E}$ (GP2) (Fig. 1). At 1200 UTC 21 January, both points are partly ice covered in the CTRL experiment, with CI concentrations of 47% and 64%, respectively. In the EXP run, the spatial gradient in CI concentration is much higher. GP1 is in the center of the northern part of the GoB, which was almost ice free in the high-resolution analysis; GP2 is characterized by almost complete ice coverage of 94%.

It has already been shown that these differences in CI result in significant differences in the turbulent fluxes and the planetary boundary layer height (Fig. 7). Vertical profiles of temperature and specific humidity for the 6-h forecast from 1200 UTC 21 January are shown

in Figs. 8a and 8b, respectively. The differences at GP1 in the vertical profiles are comparably small. Near-surface air temperature is slightly higher in the EXP run, because more open water is present. Above 800 hPa, the two curves are almost identical. The most striking difference occurs in the low-level temperature profile at GP2. The CI concentration of 93% causes a stable boundary layer up to almost 970 hPa. In the presence of 36% open water in the CTRL experiment, an unstable structure is created near the surface. The differences in near-surface air temperature are $\sim 3^\circ\text{C}$ (Fig. 8a). In addition, full ice coverage reduces the specific humidity up to a height of 900 hPa. The difference at the surface is almost 0.3 g kg^{-1} .

Atmospheric column water vapor, low cloud coverage, and total cloud coverage for both grid points are listed in Table 1. For the 6-h forecast, that is, at 1800 UTC, there are hardly any differences between the CTRL experiment and the EXP run in these parameters. The synoptic situation, with a comparably strong northerly flow (Fig. 5) and extensive cloud fields east of the Gulf of Bothnia, suggests that the lower boundary conditions have little influence on the atmospheric state. In the 18-h forecast, that is, at 0600 UTC, wind speed dropped considerably while the differences between the CTRL experiment and the EXP run in terms of temperature and specific humidity profile remain comparable to the 1800 UTC cases. This situation results in differences in low-level cloud cover of almost

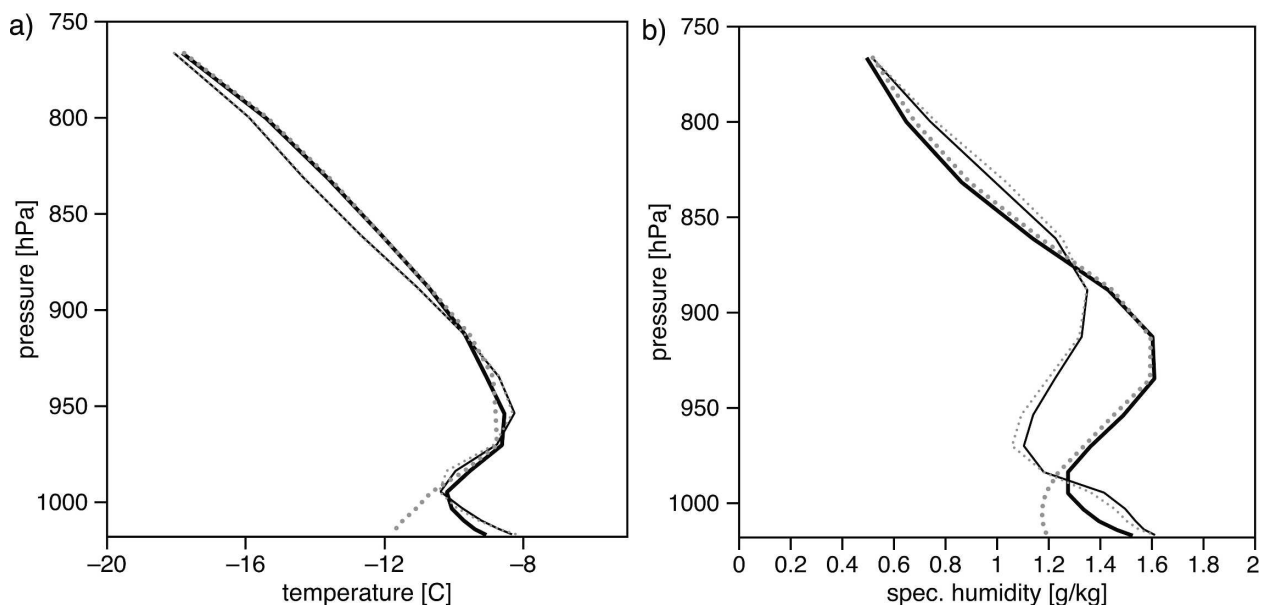


FIG. 8. Vertical profiles of (a) temperature and (b) specific humidity for GP1 ($64.4^\circ\text{N}, 22.4^\circ\text{E}$; thin lines) and GP2 ($65.1^\circ\text{N}, 24.0^\circ\text{E}$; thick lines). The values shown are the 6-h forecasts from 1200 UTC 21 January. The solid lines show data from the CTRL experiment; the dashed gray curves refer to the EXP run.

TABLE 1. Selected surface parameters at two model grid points for 21 and 22 January: sea ice concentration (CI), planetary boundary layer height (PBLH), low cloud cover (LCC), total cloud cover (TCC), and total column water vapor (TCWV). The table shows data from the 6- and 18-h forecasts. The forecast base time is 1200 UTC 21 January.

Forecast time (UTC)	Parameter	GP1 (64.4°N, 22.4°E)		GP2 (65.1°N, 24.0°E)	
		CTRL	EXP	CTRL	EXP
1800	CI (%)	47	9	64	94
	PBLH (m)	295	320	216	98
	LCC (%)	6.0	9.2	14.4	14.7
	TCC (%)	6.0	9.2	14.4	14.7
	TCWV (kg m ⁻²)	3.44	3.43	3.58	3.57
0600	CI (%)	47	9	64	94
	PBLH (m)	199	196	147	88
	LCC (%)	85.0	78.0	99.0	59.3
	TCC (%)	85.0	78.0	99.0	59.3
	TCWV (kg m ⁻²)	2.09	2.17	1.91	1.89

40% at GP2 (Table 1). Because of the lack of in situ observations, it is impossible to validate the results discussed above. However, it has been demonstrated that local differences in CI concentration affect the boundary layer and cloud coverage, even in a coarse-resolution global model.

5. Summary and discussion

The comparison of sea ice extent and mean sea ice concentration for the Baltic Sea and three subbasins as derived from the coarse-resolution NCEP dataset and the high-resolution SMHI analysis shows important differences. In general, sea ice extent from the NCEP dataset exceeds the sea ice extent analyzed at SMHI by more than 10% for the Baltic Sea. In the individual subbasins the values can be much larger. Mean sea ice concentrations agree reasonably well during the ice-growing and ice-melting periods. For the peak sea ice period during February and March the high-resolution product results in higher mean concentrations. These comparisons suggest that the spatial variability of sea ice cannot be captured accurately by the SSM/I observations. As a consequence, low sea ice concentrations are overestimated, which leads to comparably large ice extents. On the other side, high ice concentrations are underestimated so that the mean sea ice concentration is too low when compared with the high-resolution product.

The integration of the SMHI dataset into the global CI analysis is straightforward, because there is no CI transport to/from the North Sea. The differences in CI as summarized above result in significant changes in the

turbulent surface fluxes. For the 20-day period, mean differences of up to 30 W m⁻² in heat fluxes have been found for ice-free and completely ice covered areas in the high-resolution dataset. The spatially averaged 24-h mean differences of the fluxes (calculated from the EXP and CTRL runs) are of the same order of magnitude and are comparable with the temporal variability during the study period. The results presented in Figs. 2 and 4 suggest that mean sea ice extent rather than mean sea ice concentration is the determining influence on the fluxes.

It has to be ensured that the high-resolution CI analysis from SMHI does not have an adverse impact on the forecast quality. To check the forecast quality on the continental scale, anomaly correlations for the 1000- and 500-hPa levels have been computed for geopotential height and dry-bulb temperatures (Simmons et al. 1995). The correlations for northern Europe, which are based on the 60 ten-day forecasts performed during the period from 5 January to 4 March, exhibit a neutral impact. The results for 1000-hPa temperatures suggest slightly higher skills of the CTRL experiment for days 7–10. For 500-hPa temperatures, the skill scores for the EXP run are higher for days 4–7. These differences are not statistically significant, however.

On regional to local scales the differences in the forecast surface parameters (surface fluxes, temperature, humidity, and planetary boundary layer height) are nonnegligible and can influence modeled cloud coverage. For a number of practical applications, for example, icing of ships, fog forecast, air quality, and dispersion of pollutants, the differences in the planetary boundary layer can be crucial. In the future, additional work based on multiyear datasets and more observations is needed to quantify the impact of improved sea ice analyses on the medium-range weather forecast. Apart from the forecast, the sea ice concentration analysis is a useful product in itself as a comprehensive diagnostic part of the ocean–atmosphere system. For atmospheric numerical modeling applications and weather forecasting, the CI analysis has a particular value as the initial state. In addition, the CI analysis can be used for the quality check in the SST analysis.

Because ECMWF does not run a coupled ocean–sea ice–atmosphere model for the medium-range forecast, the initial sea ice conditions have to be kept constant throughout the forecast range. As was shown in this study, this necessity can have an impact on the weather parameters. The SMHI high-resolution dataset can be used to analyze the temporal variability during the forecast period. Figure 9 shows the maximum difference between the CI at the beginning of a 10-day forecast period and the values analyzed during the forecast pe-

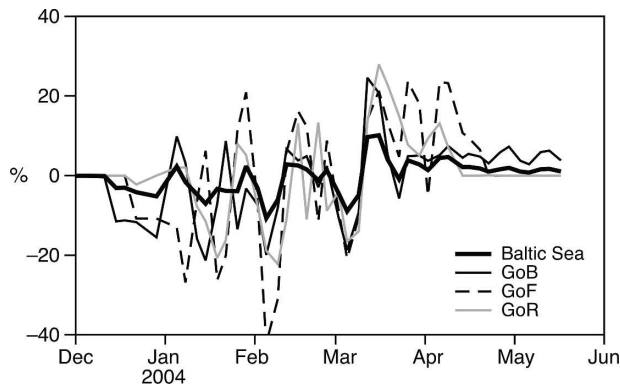


FIG. 9. Maximum differences between the mean CI concentration at the beginning of the forecast and the individual values during the consecutive 10-day forecast period. Ice concentrations have been computed from the SMHI high-resolution dataset.

riod. For all three subbasins, differences exceeding 20% occur during the 2003/04 winter season. For the Gulf of Finland a single period with a maximum difference of 40% has been detected. Based on the absolute values for the differences, mean values of 7.7% (GoB), 10.6% (GoF), 7.1% (GoR), and 3.2% (Baltic Sea) have been obtained for the season. These differences are comparable to the differences introduced through the two datasets. As a consequence, important errors in the surface fluxes can be introduced by not updating the sea ice field. Similar results have been found with high-resolution models for shorter forecast periods of up to 48 h (Gustafsson et al. 1998). It would consequently be desirable to use a coupled ocean–sea ice–atmosphere model [as described, e.g., in Meier and Döscher (2002) and Gustafsson et al. (1998)] for the weather forecast or to include offline sea ice concentration forecasts as lower boundary conditions.

Because of its shape, ragged coastline, and the large number of islands, sea ice cover in the Baltic Sea is difficult to analyze from satellite-borne passive microwave observations. Thus, the accuracy of automated global datasets like the NCEP product is limited. These difficulties are hard to overcome, even with sensors at higher resolutions, for example, the Advanced Microwave Scanning Radiometer. Operational high-resolution analysis for limited-area applications, such as the one produced by SMHI, are potentially very useful contributions that can be used together with the globally derived NCEP analysis. Similar limited-area products are available, for example, from the Norwegian Meteorological Service, but the merging of the global “first guess” and the local product will be more complex for large noncoastal sea areas—for example, the North Atlantic Ocean—for which the global field is potentially as accurate as the regional product.

Acknowledgments. The author thanks M. Köhler, P. Viterbo, E. Andersson, and A. Simmons (ECMWF) for many helpful comments and discussions. The CI data from SMHI have been provided through M. Lindskog and P. Kållberg (SMHI), and A. Bowen and R. Hine (ECMWF) helped with the final production of the figures.

REFERENCES

- Alexander, M., U. Bhatt, J. Walsh, M. Timlin, J. Miller, and J. Scott, 2004: The atmospheric response to realistic Arctic sea ice anomalies in an AGCM during winter. *J. Climate*, **17**, 890–905.
- Andersson, T., and N. Gustafsson, 1994: Coast of departure and coast of arrival: Two important concepts for the formation and structure of convective snowbands over seas and lakes. *Mon. Wea. Rev.*, **122**, 1036–1049.
- Brümmer, B., A. Kirchgässner, G. Müller, D. Schröder, J. Launiainen, and T. Vihma, 2002: The BALTIMOS (BALTEX Integrated Model System) field experiments: A comprehensive atmospheric boundary layer data set for model validation over the open and ice-covered Baltic Sea. *Bor. Environ. Res.*, **7**, 371–379.
- Campbell, W., P. Gloersen, W. Webster, T. Wilheit, and R. Ramseier, 1976: Beaufort Sea ice zones as delineated by microwave imagery. *J. Geophys. Res.*, **81**, 1103–1110.
- Cavalieri, D., P. Gloersen, and W. Campbell, 1984: Determination of sea ice parameters with the NIMBUS 7 SMMR. *J. Geophys. Res.*, **89**, 5355–5369.
- , J. Crawford, M. Drinkwater, D. Eppler, L. Farmer, R. Jentz, and C. Wackerman, 1991: Aircraft active and passive microwave validation of sea ice concentration from the Defense Meteorological Satellite Program (DMSP) Special Sensor Microwave Imager. *J. Geophys. Res.*, **96**, 21 989–22 008.
- Deser, C., J. Walsh, and M. Timlin, 2000: Arctic sea ice variability in the context of recent atmospheric circulation trends. *J. Climate*, **13**, 617–633.
- , M. Holland, G. Reverdin, and M. Timlin, 2002: Decadal variations in Labrador Sea ice cover and North Atlantic sea surface temperatures. *J. Geophys. Res.*, **107**, 3035, doi:10.1029/2000JC000683.
- Drusch, M., R. Lindau, and E. Wood, 1999: The impact of the SSM/I antenna gain function on land surface parameter retrieval. *Geophys. Res. Lett.*, **26**, 3481–3484.
- ECMWF, cited 2003: IFS documentation. [Available online at <http://www.ecmwf.int/research/ifsdocs/>.]
- Gloersen, P., and D. Cavalieri, 1986: Reduction of weather effects in the calculation of sea ice concentration from microwave radiances. *J. Geophys. Res.*, **91**, 3913–3919.
- Grumbine, R., 1996: Automated passive microwave sea ice concentration analysis at NCEP. NOAA NCEP Tech. Note 120, 13 pp. [Available online at <http://polar.ncep.noaa.gov/seaice/docs/ssmi.auto/ssmi120.html>.]
- Gustafsson, N., L. Nyberg, and A. Omstedt, 1998: Coupling of a high-resolution atmospheric model and an ocean model for the Baltic Sea. *Mon. Wea. Rev.*, **126**, 2822–2846.
- Hollinger, J., R. Poe, R. Savage, and J. Peirce, 1987: Special Sensor Microwave/Imager user’s guide. Naval Research Laboratory Tech. Rep., 120 pp.
- Hurrell, J., Y. Kushnir, G. Ottersen, and M. Visbek, 2003: *The North Atlantic Oscillation: Climate Significance and Environ-*

- mental Impact. Geophys. Monogr. Series*, No. 134, Amer. Geophys. Union, 279 pp.
- Launiainen, J., B. Cheng, J. Uotila, and T. Vihma, 2001: Turbulent surface fluxes and air-ice coupling in the Baltic Air-Sea Ice Study (BASIS). *Ann. Glaciol.*, **33**, 237–242.
- Lindau, R., 2002: Energy and water balance of the Baltic Sea derived from merchant ship observations. *Bor. Environ. Res.*, **7**, 417–424.
- , and E. Ruprecht, 2000: SSM/I-derived total vapour content over the Baltic Sea compared to independent data. *Meteor. Z.*, **9**, 117–123.
- Meier, H., and R. Döscher, 2002: Simulated water and heat cycles of the Baltic Sea using a 3D coupled atmosphere-ice-ocean model. *Bor. Environ. Res.*, **7**, 327–334.
- Raschke, E., and Coauthors, 2001: BALTEX (Baltic Sea Experiment): A European contribution to the investigation of the energy and water cycles over a large drainage basin. *Bull. Amer. Meteor. Soc.*, **82**, 2389–2413.
- Simmons, A., R. Mureau, and T. Petroligis, 1995: Error growth and estimates of predictability from the ECMWF forecasting system. *Quart. J. Roy. Meteor. Soc.*, **121**, 1739–1771.
- Slonosky, V., L. Mysak, and J. Derome, 1997: Linking Arctic sea ice and atmospheric circulation anomalies on interannual and decadal timescales. *Atmos.-Ocean*, **35**, 333–366.
- Troen, I., and L. Mahrt, 1986: A simple model of the atmospheric boundary layer; sensitivity to surface evaporation. *Bound.-Layer Meteor.*, **37**, 129–148.